

Proceedings of the XLIVth Zakopane School of Physics, Zakopane, May 18–23, 2009

# Imaging and Patterning on Nanometer Scale Using Coherent EUV Light

P.W. WACHULAK<sup>a</sup>, M.C. MARCONI<sup>b</sup>, C.S. MENONI<sup>b</sup>, J.J. ROCCA<sup>b</sup>,  
H. FIEDOROWICZ<sup>a</sup> AND A. BARTNIK<sup>a</sup>

<sup>a</sup>Institute of Optoelectronics, Military University of Technology, Gen. S. Kaliskiego 2, 00-908 Warsaw, Poland

<sup>b</sup>Electrical and Computer Engineering, Colorado State University  
1320 Campus Delivery, Engineering Res. Center, Fort Collins, CO, USA

Extreme ultraviolet (EUV) covers wavelength range from about 5 nm to 50 nm. That is why EUV is especially applicable for imaging and patterning on nanometer scale length. In the paper periodic nanopatterning realized by interference lithography and high resolution holographic nanoimaging performed in a Gabor in-line scheme are presented. In the experiments a compact table top EUV laser was used. Preliminary studies on using a laser plasma EUV source for nanoimaging are presented as well.

PACS numbers: 42.25.Hz, 42.40.Ht, 42.40.–i, 42.55.Vc

## 1. Introduction

Reaching the realm of nano-scale is very important for modern science. Much effort has been devoted to the realization of smaller, faster and less power consuming computer processors, higher density information storage, photonic crystals, etc. The idea of manipulation at the scales comparable to the sizes of molecules and even atoms was very attractive for a long time. Nanopatterning and nanoimaging are very important steps in controlling the matter on these small length scales. Nanopatterning allows for surface modifications while nanoimaging opens a possibility to “see” these features and acts as a feedback mechanism used to evaluate the results.

The direct way to improve the resolution in imaging or patterning is to use a shorter illumination wavelength. The spatial resolution given by:  $\Delta = \frac{a\lambda}{NA}$  (where  $a \in (0.3, 1)$  depending on the method used to measure the resolution and coherence of the source [1]), strongly depends on the wavelength of the illumination  $\lambda$ . The shorter the wavelength the better resolution can be attained. Another important parameter is the numerical aperture (NA) of the imaging system. Increasing the NA is a different way to improve the spatial resolution of the system.

In this paper applications of compact laboratory sources of coherent EUV radiation to nanoimaging and nanopatterning are presented. Illumination wavelength a factor of 10–100 times shorter in the EUV range makes these sources suitable for nanopatterning and high resolution imaging experiments.

## 2. Coherent EUV sources

The lack of sufficiently bright and coherent EUV sources delayed a development of EUV science and technology for many years. The development of compact,

table top coherent EUV sources: capillary discharge lasers, high harmonics generation (HHG) sources, laser-pumped EUV sources with solid, liquid and gaseous targets among others, opened the possibility to perform experiments previously restricted to large facilities. These experiments can now be performed in much smaller environments, such as university laboratories for example. Herein a very brief description of available coherent EUV sources will be presented with an emphasis on their coherence parameters due to the fact that the experiments, presented in this paper, require a spatially and temporally coherent radiation.

### 2.1. Synchrotron sources

Synchrotrons utilize a narrow confined beam of electrons or positrons that travel in a closed loop accelerated to velocities approaching the speed of light, redirected by the magnetic field and accelerated by the electric field. Charged particles under acceleration emit photons, decreasing their energy. To keep the path of the accelerated particles a small amount of energy is added in each cycle. Just as an example an undulator light from the electron storage ring Aladdin at the Synchrotron Radiation Center of the University of Wisconsin has a band width of 2.5–4% depending on the photon energies [2],  $\lambda/\Delta\lambda \approx 25$ –40 and the longitudinal coherence length is in micrometer range. Often an interferometry station or a selective optics is used to reduce the spectral band width to about  $\Delta\lambda/\lambda \approx 0.1\%$ . To have a fully spatially coherent EUV beam, micrometer size pinholes have to be used. All these coherence improving techniques are associated with serious flux reduction if these sources are to be used in interferometric experiments.

### 2.2. Free electron lasers

Both synchrotrons and free electron lasers (FEL) are large and very expensive facilities with limited user access. In the FEL a beam of electrons is accelerated to

relativistic speeds — similarly to the synchrotrons. The beam passes through a periodic, alternating transverse magnetic field. This field is produced by an assembly of magnets — the undulator, with alternating magnetic poles along the beam path that forces the beam of electrons to travel in a sinusoidal path. The acceleration due to changing the direction of the electron propagation results in releasing short wavelength photons. The example of the FEL is a FLASH source located in Hamburg, Germany. It provides a tunable wavelength 6.5–47 nm, average pulse energy  $\approx 100 \mu\text{J}$ , pulse duration 10–50 fs and spectral width of 0.5–1% [3],  $\lambda/\Delta\lambda \approx 100\text{--}200$  that leads to the longitudinal coherence length in micrometer range. The radiation has very good spatial coherence, but spectral narrowing might be necessary for specific experiments such as interferometry or holography.

### 2.3. Coherent EUV plasma sources

Coherent EUV light can be efficiently produced by amplified spontaneous emission (ASE) in an elongated plasma column with appropriate thermodynamic parameters. Lasing plasma gain media are produced by a high-current discharge in gas or by a line focusing of a high-intensity laser beam at optical or infrared wavelengths on a solid target. These approaches proved to be an efficient way to obtain a coherent EUV light and the EUV lasers, available now, can produce pulses of EUV light with time duration ranging from a few ps to a few ns with energy up to a few mJ. The detailed information on EUV lasers and their applications can be found in [4].

### 2.4. EUV sources based on high harmonic generation

HHG is a nonlinear process that involves a laser capable of producing femtosecond pulses (typically a Ti:sapphire) and a noble gas. Classically, the electric field of the ultrafast laser pulse interacts with the individual gas atoms pulling their electrons apart from the nucleus. As the electrons change their paths, de-accelerate and travel back towards the nucleus, the change in their paths results in the photon emission. Harmonics typically appear in a narrow forward radiation cone. The EUV pulses have hundreds of as to a few fs durations and the divergence half angle of the beam is usually less than  $\approx 1$  mrad [5]. These very compact sources have tunable short wavelength output and coherence similar to that of synchrotrons, high repetition rate (up to 100 kHz) and require very low maintenance as compared to large facilities. The main disadvantage is energy per pulse in nJ range. The detailed information on coherent EUV sources based on HHG and their applications can be found in [4].

## 3. Capillary discharge EUV laser

Capillary discharge EUV laser used in this work is based on creating the gain medium in a form of a long plasma channel (capillary) filled with a gas and rapid plasma excitation by a fast current discharge [6]. This

laser, developed at the Colorado State University, is based on a pulsed excitation produced by a high current pulse delivered by a discharge of a large liquid dielectric capacitor that is charged to high voltage, roughly 200 kV, by a multistage voltage amplifier — Marx generator [7, 8]. Lasing takes place in the  $3s^1P_1\text{--}3p^1S_0$  transition of Neon-like Ar by exciting Ar in an alumina capillary 3.2 mm in diameter with a current pulse having an amplitude of  $\approx 24$  kA [9]. The fast current pulse (10% to 90% rise time of  $\approx 50$  ns for 27 cm capillary length) is produced by discharging a water dielectric cylindrical capacitor through a spark gap switch connected in series with the capillary load. The current pulse rapidly compresses the plasma column to achieve a dense and hot filamentary plasma channel where a population inversion is created by strong monopole electron impact excitation of the laser upper level and rapid radiative relaxation of the laser lower level [10]. An optimum Ar gas pressure of 490 mTorr was maintained in the capillary channel to produce  $\approx 0.15$  mJ laser pulses with half angle divergence of 4.5 mrad at a repetition rate of 1 Hz. The laser beam has very high spatial and temporal coherence. The longitudinal coherence length of  $\approx 470 \mu\text{m}$  is determined by the line width that is mainly limited by the Doppler broadening of the laser transition [11]. The capillary with a length of 27 cm used in this experiment generates a laser beam that has a spatial coherence radius of approximately  $570 \mu\text{m}$  measured at the experiment chamber located at 1.7 m from the exit of the laser [12]. The coherence properties of capillary discharge laser (CDL) make this unique source very suitable for nanopatterning using interference lithography (IL) and EUV holography.

## 4. Nanopatterning with EUV laser

Patterning of sub-60 nm features in the photoresist surface using coherent EUV light produced by the capillary discharge laser was realized utilizing an IL technique [13]. The IL technique was implemented by illuminating a flat mirror in the Lloyd configuration with the EUV laser output. In this configuration, part of the laser beam impinges on the mirror at a grazing incidence angle  $\theta$  and is reflected and overlapped with the remaining un-deflected part of the beam, as shown schematically in Fig. 1b. Beam interference produces a sinusoidal intensity pattern with period  $d = \frac{\lambda}{2\sin(\theta)}$ , defined by the wavelength of the light  $\lambda$  and the incidence angle  $\theta$ . Figure 1a shows a 3D schematic of the setup used for nanometer scale nanopatterning. A rectangular  $30 \times 50 \text{ mm}^2$  Cr coated flat mirror was mounted at grazing incidence in front of the laser beam on a motorized pivoting platform. The sample — Si wafer coated with 30 nm thick polymethyl methacrylate (PMMA) layer, was mounted at the edge of the mirror in a motorized rotation stage that allows for multiple exposures with variable angle between the exposures  $\alpha$ . A translation stage retracts the sample from the mirror edge before each rotation. The Lloyd mirror interferometer system was housed in a vacuum chamber

$0.45 \times 0.55 \times 0.40 \text{ m}^3$  differentially pumped to maintain a pressure of approximately  $10^{-5}$  Torr. The entire EUV nanopatterning instrument has a footprint of  $0.7 \times 2.6 \text{ m}^2$ .

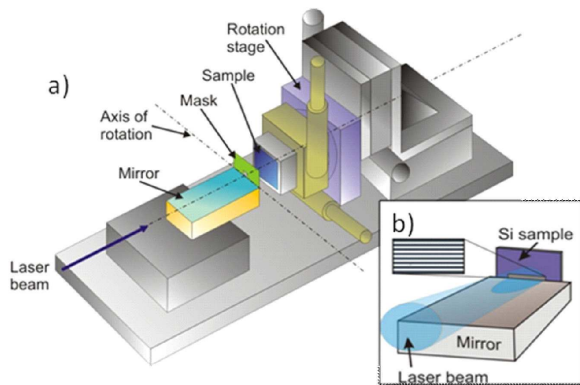


Fig. 1. (a) 3D schematic of the compact nanopatterning tool based on Lloyd's mirror interferometer, (b) scheme of the mirror illumination and producing the interference pattern at the sample plane.

Typical exposure times of 30–50 s (30–50 laser pulses) were necessary to print periodic patterns up to  $500 \times 500 \mu\text{m}^2$  area. Thickness of 30 nm was matched with the penetration depth of the 46.9 nm photons in PMMA, allowing the photolithographic pattern to reach the substrate. This was accomplished by spin coating the substrate with diluted 1% PMMA in anisole at 5000 rpm in a standard spin coater. After the exposure the PMMA was developed using standard procedure consisting of immersion in a 1:3 solution of methyl isobutyl ketone (4-methyl-2-pentanone) (MIBK) with isopropyl alcohol (IPA) for 35 s, followed by rinsing with IPA. The sample was subsequently dried using compressed nitrogen.

If an applied dose was  $166 \text{ mJ}/\text{cm}^2$  at the sample plane a regular array of small non-activated spots, at the intersections of two exposed 1D patterns, was produced after the resist developing procedure. Figure 2a shows the experimental pattern obtained using an atomic force microscope (AFM) that corresponds to a very regular array of cone-shaped dots. The period, 150 nm in this example, can be continuously changed by varying the grazing incidence angle  $\theta$ . The FWHM of the features is approximately 60 nm. If the angle between the exposures was changed from  $\alpha = \pi/2$  to  $\pi/4$  the pillars on hexagonal grid can be fabricated as shown in Fig. 2b.

Similar patterns were fabricated in hydrogen silsesquioxane (HSQ) photoresist [14]. The advantage of this inorganic resist, as compared with carbon-based photoresists, is its lower attenuation in the EUV region. After the exposure the Si samples coated with  $\approx 150 \text{ nm}$  thick HSQ layer were post-baked for 15 min at  $110^\circ\text{C}$ . The developing was performed in LDD26W, 2.38% tetra-methyl-ammonium hydroxide (TMAH) in water for 45 s, rinsed with de-ionized water and dried with nitrogen gas. Figure 3a shows a result of single exposure with  $\approx 100 \text{ nm}$  FWHM wide grooves fabricated in the

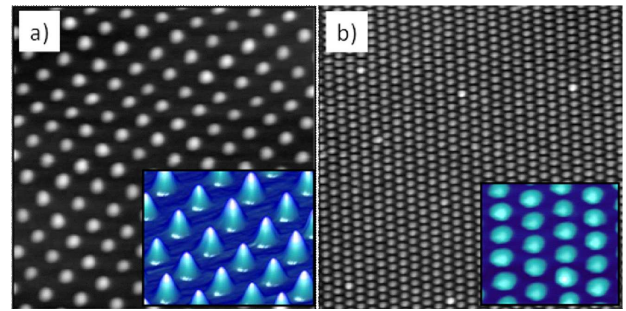


Fig. 2. AFM scans of the surface of PMMA photoresist after multiple exposures with Lloyd's mirror interferometer showing (a) pillars 58 nm diameter, scan size  $2 \times 2 \mu\text{m}^2$ , with the angle between the exposures equal to  $\alpha = \pi/2$  and (b) pillars 130 nm diameter, scan size  $10 \times 10 \mu\text{m}^2$ , with the angle between the exposures equal to  $\alpha = \pi/4$ .

HSQ photoresist. In double exposure scheme if the exposure dose was equal to  $14 \text{ mJ}/\text{cm}^2$  the photoresist is only activated in small volumes in the intersections of the fringes corresponding to the maxima of interference, developing in this case an array of small pillars-dots, as shown in Fig. 3b. For  $\approx 55 \text{ mJ}/\text{cm}^2$  the resist is activated in wide strips that develop in the intersections small holes. Figure 3c shows a  $4 \times 4 \mu\text{m}^2$  section of the array of holes 100 nm FWHM and 120 nm deep patterned in the HSQ surface.

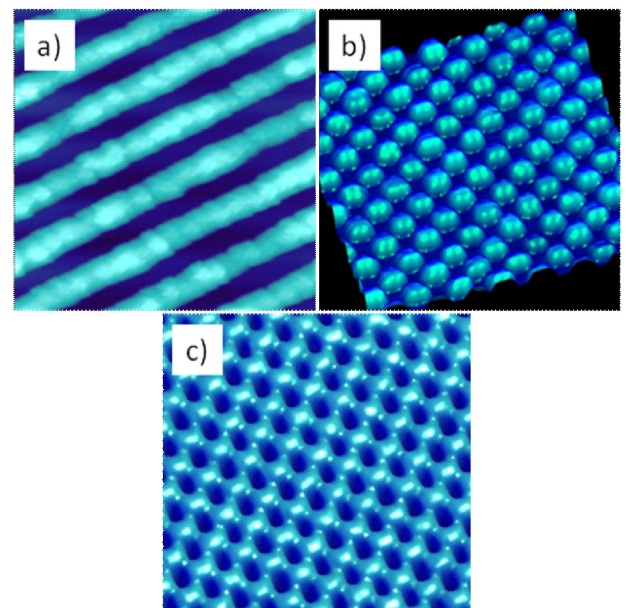


Fig. 3. AFM scans of the surface of HSQ photoresist after single and multiple exposures with Lloyd's mirror interferometer showing (a) 100 nm wide grooves, scan size  $2.5 \times 2.5 \mu\text{m}^2$ , (b) pillars 200 nm in diameter, scan size  $4 \times 4 \mu\text{m}^2$ , with the angle between the exposures equal to  $\alpha = \pi/2$  and (c) 100 nm diameter holes,  $\approx 120 \text{ nm}$  depth, scan size  $4 \times 4 \mu\text{m}^2$ .

The versatility of this IL set up allows changing the features (holes or dots) very easily by changing the applied photon flux and the periodicity by changing the incidence angle on the mirror  $\theta$ . The size and distribution of the holes and nanodots in the array were very homogeneous and uniform throughout the patterning area of  $0.5 \times 0.5 \text{ mm}^2$ .

### 5. High resolution holographic imaging with EUV laser

The ability to acquire sub-50 nm resolution reconstructions of the holograms of nanoscale objects illuminated by a compact, table-top light source represents a significant contribution to nanoscience and nanotechnology as an alternative imaging scheme next to the visible light microscopy, AFM microscopy or SEM. To show the possibility of sub-50 nm hologram recording and reconstruction an object composed of carbon nanotubes (CNT) (50–80 nm in diameter 10–20  $\mu\text{m}$  in length) placed on a 100 nm thick silicon membrane was imaged using a table top EUV laser in a Gabor in-line configuration shown in Fig. 4a [15].

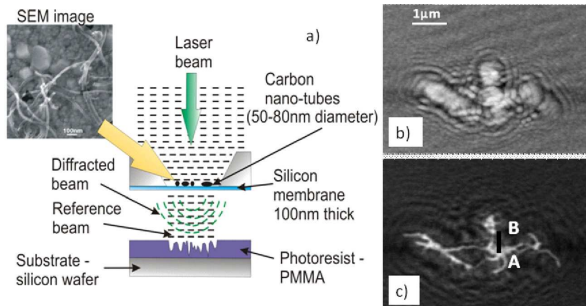


Fig. 4. (a) Scheme of Gabor's in-line holographic configuration for hologram recording, (b) a portion of the hologram stored in the photoresist surface scanned with AFM, (c) image reconstructed using Fresnel propagator algorithm with a line indicating a cut for knife-edge resolution assessment.

Thin Si membrane has a 60% transparency at  $\lambda = 46.9 \text{ nm}$  [16] and acts as a support for the object. The object was placed at  $\approx 2.6 \mu\text{m}$  away from a 120 nm thick PMMA layer of photoresist spun on a Si wafer. Limited area of hologram digitization with the AFM ( $9.9 \times 9.9 \mu\text{m}^2$ ) reduces the effective NA of digitization to 0.88, and resolution based on the Rayleigh criterion to 26.7 nm. The object was illuminated by a compact EUV laser, described in Sect. 3, and the hologram recorded as a relief modulation in the surface of the photoresist was developed in MIBK:IPA 1:3 solution for 30 s. Later the AFM was used to generate digitized versions of the holograms that were reconstructed by numerically simulating the illumination with a readout wave. The amplitude and the phase distribution of the field in the image plane were obtained calculating the field emerging from the hologram illuminated by a plane reference wave

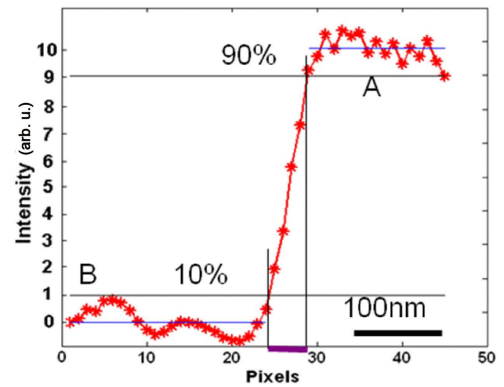


Fig. 5. Knife-edge resolution measurement showing 10–90% intensity transition over  $\approx 46 \text{ nm}$ .

and numerically back-propagating the field with a Fresnel propagator [17].

Figure 4b shows a hologram digitized with the AFM. The corresponding numerical reconstruction processed with a Fresnel propagation code is shown in Fig. 4c. The CNTs are clearly distinguishable as white lines. The spatial resolution in the reconstructed image was evaluated using the knife-edge method based on measuring the 10–90% rise of the intensity in line-cut, shown in Fig. 5, (A–B line in Fig. 4c) through the image. To properly recreate the knife edge resolution test this cut was realized in a region where a “plateau” in the maximum and minimum intensities was clearly reached. An average of similar cuts realized in different points of the image results in a resolution of  $45.8 \pm 1.9 \text{ nm}$  where the error is assigned by the standard deviation spread in the measurements. These measurements were confirmed using a Gaussian filtering and correlation method described in more detail in [18].

### 6. Future plans

The experiments in nanoimaging and nanopatterning with the use of a capillary discharge EUV laser performed at the Colorado State University will be continued at the Military University of Technology using a compact laser plasma EUV source based on a gas puff target [19] and a laser-driven source based on high harmonic generation. A high resolution EUV microscope has been designed and it is currently under development for imaging with nanometer resolution. In the microscope the diffraction optics — Fresnel zone plates with outer zone widths of 50 and 100 nm will be utilized for imaging of an object with high magnification and sub-100 nm resolution. The object is illuminated with quasi-monochromatic EUV light produced from a laser-irradiated argon gas puff target and then focused and spectrally filtered by an ellipsoidal multilayer mirror with Mo/Si coating. Schematic of the EUV microscope is shown in Fig. 6. The research is in progress. Preliminary results have shown the possibility to obtain EUV images.

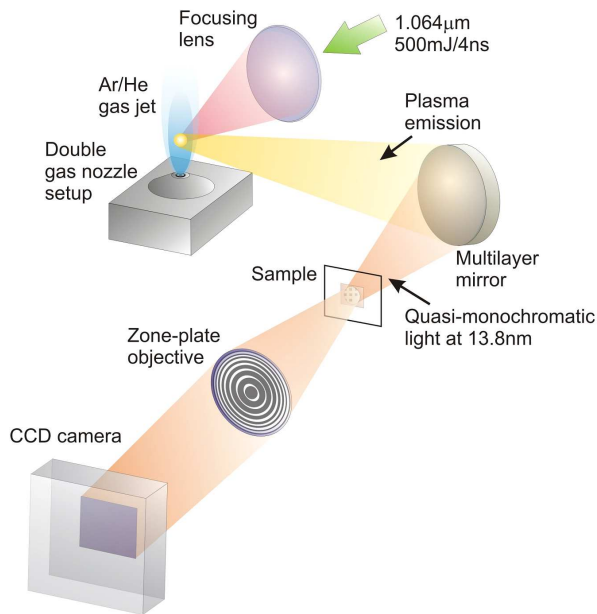


Fig. 6. Schematic of the EUV microscope with a laser plasma source based on a gas puff target.

It is also planned to perform the holographic nano-imaging using a HHG source pumped by a high-intensity femtosecond Ti:sapphire laser system. The laser system with appropriate parameters to generate high harmonics in the EUV range has been recently installed at the Institute of Optoelectronics. For the experiments a special elongated gas puff target has been developed at the Military University of Technology. The target was used for generation of bright and low divergence high harmonics in the collaborative experiments [19, 20].

## 7. Conclusions

In conclusion, the results obtained at CSU show that the EUV laser combined with IL schemes has a potential to become a useful compact alternative for printing nanometer features in a simple and versatile way. Short wavelength of the EUV laser enables a sub-50 nm holographic imaging and may become a photon based, high resolution imaging method complimentary to scanning electron microscopy and atomic force microscopy especially with further development of shorter wavelength EUV sources. New existing and future EUV sources at MUT may also substantially contribute to the high resolution EUV imaging in the near future.

## References

- [1] J.M. Heck, D.T. Attwood, W. Meyer-Ilse, E.H. Anderson, *J. X-ray Sci. Technol.* **8**, 95 (1998).
- [2] H.H. Solak, D. He, W. Li, F. Cerrina, *J. Vac. Sci. Technol. B* **17**, 6 (1999).
- [3] [http://flash.desy.de/sites/site\\_vuvfel/content/e395/e2188/FLASH-Broschrefrs\\_web.pdf](http://flash.desy.de/sites/site_vuvfel/content/e395/e2188/FLASH-Broschrefrs_web.pdf), as in June 2009.
- [4] P. Jaeglé, *Coherent Sources of XUV Radiation, Soft X-ray Lasers and High-Order Harmonic Generation*, Springer Series in Optical Sciences, Vol. 106, 2006.
- [5] D. Attwood, *Soft X-rays and Extreme Ultraviolet Radiation: Principles and Applications*, Cambridge Univ. Press, Cambridge 1999.
- [6] B.R. Benware, C.D. Macchietto, C.H. Moreno, J.J. Rocca, *Phys. Rev. Lett.* **81**, 5804 (1998).
- [7] J.J. Rocca, D.P. Clark, J.L.A. Chilla, V.N. Shlyaptsev, *Phys. Rev. Lett.* **77**, 1476 (1996).
- [8] A. Ritucci, G. Tomassetti, A. Reale, L. Palladino, L. Reale, F. Flora, L. Mezi, S.V. Kukhlevsky, A. Faenov, T. Pikuz, *Appl. Phys. B* **78**, 965 (2004).
- [9] C.D. Macchietto, B.R. Benware, J.J. Rocca, *Opt. Lett.* **24**, 1115, (1999).
- [10] J.J. Rocca, V.N. Shlyaptsev, F.G. Tomasel, O.D. Cortazar, D. Hartshorn, J.L.A. Chilla, *Phys. Rev. Lett.* **73**, 2192 (1994).
- [11] Y. Liu, M. Seminario, F.G. Tomasel, C. Chang, J.J. Rocca, D.T. Attwood, *Phys. Rev. A* **63**, 033802 (2001).
- [12] Y.W. Liu, M. Seminario, F.G. Tomasel, C. Chang, J.J. Rocca, D.T. Attwood, *J. Phys. IV (France)* **11**, 123, (2001).
- [13] P.W. Wachulak, M.G. Capeluto, M.C. Marconi, C.S. Menoni, J.J. Rocca, *Opt. Express* **15**, 3465 (2007).
- [14] P.W. Wachulak, M.G. Capeluto, M.C. Marconi, D. Patel, C.S. Menoni, J.J. Rocca, *J. Vac. Sci. Technol. B* **25**, 2094, (2007), this article was also published in *Virtual Journal of Nanoscale Science & Technology* **16**, 26 December 24, (2007).
- [15] P.W. Wachulak, M.C. Marconi, R.A. Bartels, C.S. Menoni, J.J. Rocca, *J. Opt. Soc. Am. B* **25**, 1811 (2008).
- [16] CXRO, <http://www-cxro.lbl.gov/>.
- [17] U. Schnars, W.P.O. Juptner, *Measur. Sci. Technol.* **13**, R85 (2002).
- [18] P.W. Wachulak, C.A. Brewer, F. Brizuela, W. Chao, E. Anderson, R.A. Bartels, C.S. Menoni, J.J. Rocca, M.C. Marconi, *J. Opt. Soc. Am. B* **25**, B20, (2008), this article was also published in *Virtual Journal for Biomedical Optics* **3**, 8 (2008).
- [19] D.G. Lee, H.T. Kim, K.H. Hong, C.H. Nam, I.W. Choi, A. Bartnik, H. Fiedorowicz, *Appl. Phys. Lett.* **81**, 3726 (2002).
- [20] H.T. Kim, I.J. Kim, V. Tosa, C.M. Kim, J.J. Park, Y.S. Lee, A. Bartnik, H. Fiedorowicz, C.H. Nam, *IEEE J. Select. Top. Quantum Electron.* **10**, 1329 (2005).